Bull. Chem. Soc. Jpn., 73, 1735—1748 (2000)

Headline Articles

Substituent Effect on Organotin Tp* Compounds as the Tp* Reagent for the Preparation of Mono Tp* Complexes of Group 4—6 Metals (Tp* = Tris(3,5-dimethylpyrazol-1-yl)hydroborate)

Toshiyuki Oshiki, Kazushi Mashima,* Shin-ichi Kawamura, Kazuhide Tani,* and Kazuo Kitaura*,†

Department of Chemistry, Graduate School of Engineering Science, Osaka University, Toyonaka, Osaka 560-8531

†Department of Chemistry, College of Integrated Arts and Sciences, Osaka Prefecture University, Sakai, Osaka 599-8531

(Received March 15, 2000)

Organotin compounds [Tp*$SnCl_{3-n}Bu_n$] (**2**: $n = 1$; **3**: $n = 2$) having a Tp* ligand (Tp* = tris(3,5-dimethylpyrazol-1-yl)hydroborate) are useful reagents for introducing a Tp* ligand on Group 4 and 5 metals and chromium. The test reactions of these organotin compounds along with [Tp*$SnCl_3$] (**1**) with $ZrCl_4$, affording a known complex [Tp*$ZrCl_3$] (**4**), were examined. The reaction rates were in the order **3** > **2** ≫ **1**. This tendency was understood by the average Sn–N(Tp* ligand) bond distance being longer in the order **3** > **2** > **1** as revealed by the crystallographic studies and the orbital interactions between the Tp* ligand and the $SnCl_{3-n}Bu_n$ fragments estimated by the ab initio calculations for **1**—**3**. On the basis of the above findings, we applied the compound **3** to prepare Tp* complexes of Group 4—6 metals. Reactions of $TiCl_4$ with an equimolar amount of **3** afforded [Tp*$TiCl_3$] (**7**) in good yields after a simple rinse to remove the resulting tin compound, $SnBu_2Cl_2$. [Tp*$HfCl_3$] (**8**) was prepared in moderate yield by reaction of [$HfCl_4(THF)_2$] with **3** under severe conditions. Similarly, the reactions of **3** with a stoichiometric amount of [$NbCl_4(THF)_2$] or [$NbCl_5(OEt)_2$] and $TaCl_5$ in toluene gave [Tp*$NbCl_3$] (**9**) and [Tp*$TaCl_3$][$TaCl_6$] (**10**), respectively. We also applied our synthetic method to prepare Tp* complexes of vanadium, [Tp*VCl_2(THF)] (**11**), [Tp*VCl_2(DNAP)] (**12**) (DMAP = 4-dimethylaminopyridine), and [Tp*VCl_2(=$NC_6H_3Me_2$-2,6)] (**13**) and those of chromium, [Tp*$CrCl_2$(L)] (**14**: L = THF; **15**: L = H_2O; **16**: L = DMAP). Some of these Tp* complexes, **4**, **8**, **12**, **13**, **15**, and **16** were crystallographically characterized to have discrete octahedral geometry containing the facial coordination of the Tp* ligand.

Tris(pyrazol-1-yl)hydroborate (= Tp) and its derivatives typically serve as tridentate mono anionic six-electron donor ligands,[1—3] which are isoelectronic to cyclopentadienyl ligands. Moreover, the Tp ligand provides a sterically hindered coordination environment.[4,5] The transition metal complexes bearing the Tp ligand have mostly been prepared by the metathesis reactions of metal halide compounds with an alkali metal Tp compound such as NaTp. In contrary to the successful synthesis of mono Tp complexes of late transition metals, the preparation of Tp complexes of early transition metals has been less investigated because of disadvantages of metathesis reaction; contamination of inseparable by-products, such as NaCl, hampered the isolation of a pure product and, in some cases, unexpected reduction of the starting compounds resulted in a complex mixture.[1—5] For the synthesis of the Tp complexes of early transition metals, mutual synthetic approaches by increasing the solubility of the Tp ligand and the starting halometal compounds have been examined. Introduction of a bulky alkyl substituent such as a *t*-butyl group at the 3-position of the pyrazol-1-yl ring afforded mono Tp complexes of early transition metals.[6] On the other hand, alkyl, alkylidene, alkoxide, and alkyne complexes have been used as starting compounds for the preparation of mono Tp complexes of Group 5 metals; the reactions of Me_3TaCl_2, [Ta(=CHCMe$_3$)$Cl_3(THF)_2$], and [$NbCl_3(OMe)_2]_2$ with KTp* (Tp* = tris(3,5-dimethylpyrazol-1-yl)hydroborate) have been reported to give [Tp*$TaMe_3Cl$],[7,8] [Tp*Ta(=CHCMe$_3$)Cl_2],[9] and [Tp*Nb(O)Cl(OMe)],[10] respectively, and Tp* niobium alkyne complexes have also been prepared.[11—15]

An organosilicon compound such as Cp*$SiMe_3$ (Cp* = η^5-pentamethylcyclopentadienyl) has been employed for preparing mono Cp* complexes of early transition metals;[16,17] however, the corresponding organosilicon derivatives of Tp*, which are expected to be reagents for the preparation of mono Tp* complexes, have not been isolated to date due to their thermal instability.[18] Since a Cp* organotin compound such as Cp*$SnBu_3$ has also been used as the Cp* transfer reagent, we found that a organotin compound, [Tp*$SnClBu_2$] was a practical Tp* transfer reagent for Group

4, 5, and 6 metals after systematical investigation on the organotin compounds containing the Tp* ligand. A part of this work was the subject of a preliminary communication.[19]

Results and Discussion

Reaction of $[Tp^*Sn(Cl)_{3-n}Bu_n]$ ($n = 0, 1, 2$) with $ZrCl_4$. In order to find a better reagent for introducing a Tp* ligand onto Group 4, 5, and 6 metals, we examined the reaction of equimolar amounts of $ZrCl_4$ and an organotin compound of general formula $[Tp^*SnCl_{3-n}Bu_n]$ (**1**: $n = 0$; **2**: $n = 1$; **3**: $n = 2$) as a test for the preparation of the known compound $[Tp^*ZrCl_3]$ (**4**)[20] (Eq. 1) (Chart 1). These tin compounds were prepared by the reactions of KTp* with the corresponding organotin compounds.[21]

$$\underset{\mathbf{1-3}}{Tp^*SnCl_{3-n}Bu_n} + ZrCl_4 \xrightarrow{CDCl_3} \underset{\mathbf{4}}{\text{[Tp*ZrCl}_3\text{]}} + SnCl_{4-n}Bu_n \qquad (1)$$

The reactions of **2** and **3** with a stoichiometric amount of $ZrCl_4$ at room temperature were monitored by NMR spectroscopy. Each reaction gave **4** in quantitative yield after 10 min. The same reactions at -10 °C for 10 min gave **4** in 38% yield from **2** and in 65% yield from **3**, respectively, indicating that **3** is superior to **2** as the Tp*-transfer reagent. In sharp contrast, the reaction of $ZrCl_4$ with the trichloro complex **1** did not give **4** at all under the same conditions. The reactivity of these organotin compounds sensitively depends on the number of the alkyl substituent on a tin metal; the reactivity increased with the increase of the number of the alkyl substituent. A trialkyl organotin compound such as $[Tp^*SnBu_3]$ (**5**) might be expected to be more reactive than **3**, but the compound **5**, which was derived from the reaction of KTp* and Bu_3SnCl, was thermally too unstable even in the solid state to use as the reagent. This is consistent with the reported tendency that some Tp trialkyltin compounds decomposed in solution.[22,23] As a result, we chose **3** as the reagent for the preparation of Tp* complexes of early transition metals.

Crystal Structures of Compounds 1—3. In order to get an insight into the reason why the compound **3** is superior to the other tin compounds for the introduction of the Tp* ligand, crystal structures of these tin compounds **1**—**3** were determined by X-ray analysis (Figs. 1, 2, and 3). The selected bond distances and angles are given in Table 1. We already reported the preliminary structure of the compound **3**, which was refined as minimizing the F function;[19] however, the structure of compound **3** together with those of compounds **1** and **2** were refined using F^2 function. These compounds have a discrete pseudo octahedral geometry comprised of the organotin $SnCl_{3-n}Bu_n$ ($n = 0$, 1, 2) fragment and the

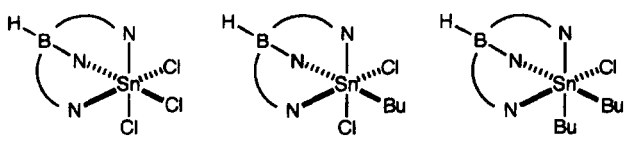

Chart 1.

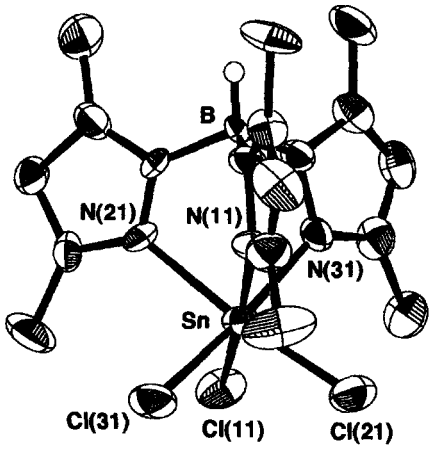

Fig. 1. ORTEP drawing of **1** with the numbering scheme. Hydrogen atoms are omitted for clarity.

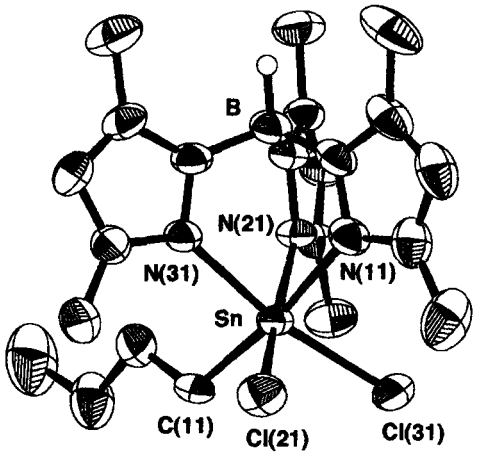

Fig. 2. ORTEP drawing of one of two crystallographically independent **2** with the numbering scheme. Hydrogen atoms are omitted for clarity.

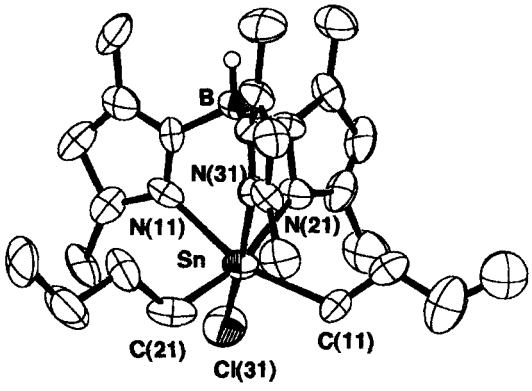

Fig. 3. ORTEP drawing of **3** with the numbering scheme. Hydrogen atoms are omitted for clarity.

Table 1. Selected Bond Distances and Angles for **1**—**3**[a)]

	1	**2-I**[b)]	**2-II**[b)]	**3**
		Bond distances (Å)		
Sn–N(11)	2.12(1)	2.224(4)	2.230(3)	2.33(2)
Sn–N(21)	2.27(1)	2.247(4)	2.268(4)	2.34(2)
Sn–N(31)	2.195(3)	2.280(4)	2.271(4)	2.287(4)
av. Sn–N	2.20	2.250	2.256	2.32
Sn–L(11)	2.397(4)	2.162(4)	2.151(4)	2.27(2)
Sn–L(21)	2.346(5)	2.424(1)	2.4372(15)	2.05(2)
Sn–L(31)	2.387(1)	2.437(2)	2.4454(15)	2.492(2)
		Bond angles (deg)		
N(11)–Sn–N(21)	83.7(1)	79.9(1)	79.4(1)	74.6(2)
N(11)–Sn–N(31)	83.5(5)	80.7(1)	80.4(1)	82.0(6)
N(11)–Sn–L(11)	171.9(3)	171.8(2)	172.0(2)	159.9(7)
N(11)–Sn–L(21)	91.7(4)	88.6(1)	88.1(1)	90.0(8)
N(11)–Sn–L(31)	90.3(4)	88.7(1)	88.7(1)	89.8(5)
N(21)–Sn–N(31)	84.8(5)	85.8(1)	85.8(1)	83.8(6)
N(21)–Sn–L(11)	89.8(4)	94.4(2)	94.3(2)	86.4(7)
N(21)–Sn–L(21)	173.8(4)	168.4(1)	167.19(9)	164.6(9)
N(21)–Sn–L(31)	91.5(4)	90.3(1)	90.2(1)	86.9(5)
N(31)–Sn–L(11)	91.2(4)	93.1(2)	94.4(2)	89.8(8)
N(31)–Sn–L(21)	90.6(4)	90.3 (1)	89.5(1)	94.5(9)
N(31)–Sn–L(31)	173.1(2)	169.2(1)	169.0(1)	168.9(2)
L(11)–Sn–L(21)	94.43(5)	96.8(1)	98.0(1)	109.0(3)
L(11)–Sn–L(31)	94.6(2)	97.3(1)	96.1(1)	95.6(6)
L(21)–Sn–L(31)	92.7(2)	91.55(5)	92.15(5)	92.9(7)

a) **1**, L(11) = Cl(11), L(21) = Cl(21), and L(31) = Cl(31); **2**, L(11) = C(11), L(21) = Cl(21), and L(31) = Cl(31); **3**, L(11) = C(11), L(21) = C(21), and L(31) = Cl(31). b) Two crystallographically independent molecules (**2-I** and **2-II**) of the complex **2** crystallize in a unit cell.

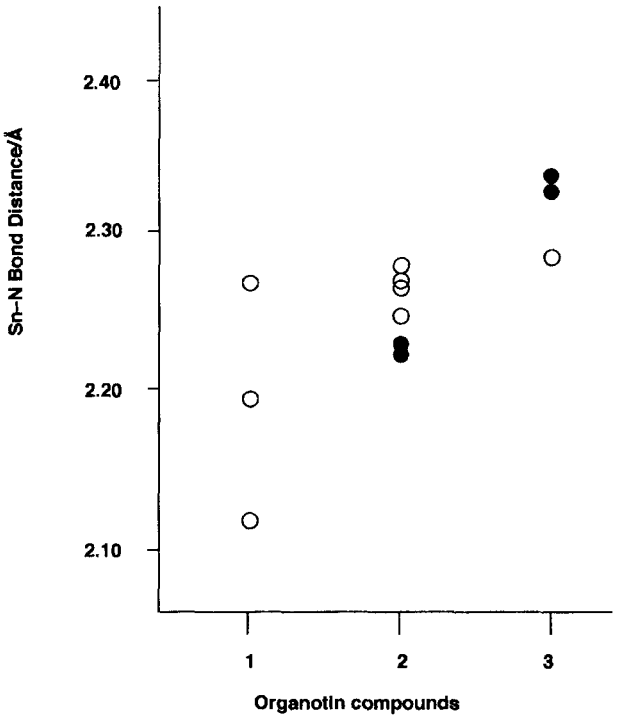

Fig. 4. The Sn–N distances (Å) of compounds **1**, **2**, and **3** vs. the number of butyl substituents. Circle (○) and solid circle (●) represent the Sn–N bond *trans* to the chloride ligand and that *trans* to the butyl group, respectively.

Tp* ligand. The unit cell of **2** contains two crystallographically-independent molecules (**2-I** and **2-II**), both of which have the same structure without any exceptional geometrical difference (Table 1).

A noteworthy structural feature of **1**—**3** appears in the Sn–N(Tp* ligand) bond distance, which changes depending on the number of the butyl substituents on the tin atom, as shown in Fig. 4. The average Sn–N bond distance is longer in the order: **1** (av. 2.20 Å) < **2** (av. 2.250 Å for molecule **2-I** and av. 2.256 Å for molecule **2-II**) < **3** (av. 2.32 Å). This order is in good accordance with general propensity that higher alkyl substituted tin compounds bearing a Tp or its derivative have much longer Sn–N bonds due to the *trans* influence of alkyl ligand(s) as σ-donor.[18,22—28] An extremely long Sn–N bond (2.388(1) Å) has been reported for a permethyltin complex, [TpSnMe$_3$].[23]

In the compound **3**, two Sn–N bond distances (2.33(2) and 2.34(2) Å) *trans* to the butyl group are longer than that (2.287(4) Å) *trans* to the chloro atom. This deviation around the Sn atom accordingly resulted in the obtuse angles of N(11)–Sn–C(11) (159.9(7)°) and N(21)–Sn–C(21) (164.6(9)°). In sharp contrast to the case of **3**, the complex **2** has the shorter Sn–N(11) bond distance (2.224(4) Å for **2-I** and 2.230(3) Å for **2-II**) *trans* to the butyl ligand than those (2.247(4)—2.280(4) Å) of Sn–N(21) and Sn–N(31) *trans* to the chloride ligand. A similar trend has also been observed in other mono aryl substituted organotin complexes such as Tp′SnPhCl$_2$ (Tp′ = tris(3-methylpyrazol-1-yl)hydro-

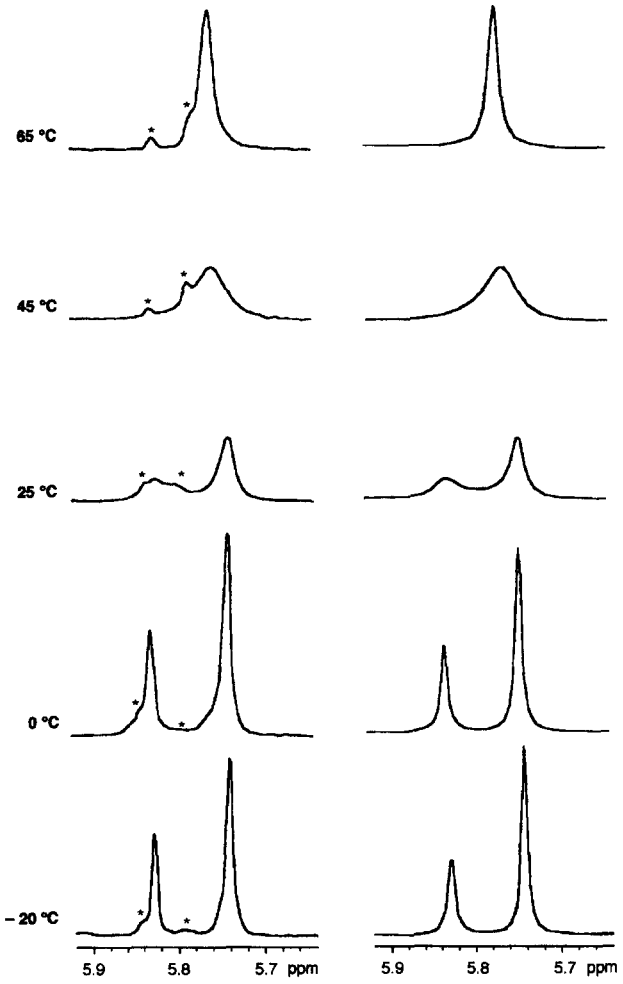

Fig. 5. Experimental (left) and calculated (right) line shapes for 270 MHz ^{1}H NMR spectra of the methine protons of the Tp* ligand in **3** in $CDCl_3$. The asterisk marks the signals due to impurities.

borate and tris(5-methylpyrazol-1-yl)hydroborate).[22,24] MO calculations can rationalize this opposite tendency (vide infra).

Variable-Temperature ^{1}H NMR Study of 3. Compound **3** in $CDCl_3$ exhibited temperature dependence in ^{1}H NMR spectroscopy, while the NMR spectra of **1** and **2** in $CDCl_3$ did not show any temperature dependence in the temperature region between −60 °C and 60 °C. The ^{1}H NMR spectra of the methine protons of the Tp* ligand of **3** at various temperatures and their computer-simulated patterns are shown in Fig. 5. At low temperature (below −20 °C), two methine signals (δ = 5.74 and 5.83) were displayed in a 2 : 1 ratio. These two signals broadened above 0 °C, coalesced around 30 °C, and then turned a singlet at δ = 5.76 at 65 °C; the spectral simulation for the methine signals gave the activation parameters for **3** to be $\Delta G^{\ddagger}$(297 K) = 16±1 kcal mol^{-1}, $\Delta H^{\ddagger}$ = 17±1 kcal mol^{-1} and $\Delta S^{\ddagger}$ = 4±2 eu. We measured the temperature-dependent ^{119}Sn NMR of **3** in $CDCl_3$ between −20 and 60 °C; however only a sharp singlet signal was observed at the whole temperature range with a slight chemical shift change from δ = −352.0 at −20 °C to δ = −348.4 at 60 °C; these chemical shift values are in accordance with a 6-coordinated tin species, but not with a 5-coordinated tin species such as **6** (Chart 2). Thus, the fluxional character of **3** is rationalized by a simple rotation around the B–Sn axis. The internal rotation around the B–metal axis has been observed for Tp complexes of molybdenum.[29–31]

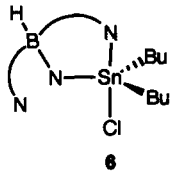

6

Chart 2.

Table 2. Selected Optimized Geometrical Parameters and Net Charge on the Tin Atom of **1**—**3** from the Ab Initio and the MNDO Calculations[a,b]

	1	2	3
		Bond distances (Å)	
Sn(1)–N(11)	2.197 (2.238)	2.217 (2.254)	2.292 (2.358)
Sn(1)–N(21)	2.197 (2.233)	2.245 (2.316)	2.292 (2.358)
Sn(1)–N(31)	2.197 (2.236)	2.245 (2.322)	2.277 (2.398)
av. Sn(1)–N	2.197 (2.236)	2.236 (2.297)	2.287 (2.371)
Sn(1)–L(11)	2.422 (2.345)	2.191 (2.193)	2.212 (2.158)
Sn(1)–L(21)	2.422 (2.346)	2.470 (2.362)	2.212 (2.158)
Sn(1)–L(31)	2.422 (2.346)	2.470 (2.362)	2.516 (2.376)
		Bond angles (deg)	
N(11)–Sn–L(11)	173.4 (171.5)	174.7 (170.6)	168.1 (161.3)
N(21)–Sn–L(21)	173.4 (167.3)	169.8 (165.0)	168.1 (161.3)
N(31)–Sn–L(31)	173.4 (169.3)	169.8 (167.0)	168.8 (170.3)
		Net charge on tin	
	+1.782 (+1.023)	+1.844 (+0.875)	+1.878 (+0.778)

a) In the parentheses are given the values obtained from the MNDO calculations. b) **1**, L(11) = L(12) = L(31) = Cl; **2**, L(11) = C and L(21) = L(31) = Cl; **3**, L(11) = L(21) = C and L(31) = Cl. See Figs. 1, 2, and 3 for the numbering scheme.

Ab initio MO Calculations of $[Tp^*Sn(Cl)_{3-n}Bu_n]$ ($n = 0$, 1, and 2). The ab initio MO calculations were performed on compounds **1**—**3** to study the effect of alkyl substitutions on the structures. The geometry optimizations of the organotin compounds were carried out at the HF/3-21G* level of wave function using the Gaussian 94 program.[32] The calculated bond lengths, bond angles, and net charges on tin atom of **1**—**3** are summarized in Table 2, together with those from the MNDO calculations. The calculated geometries of **1**, **2**, and **3** have C_{3v}, C_s, and C_s symmetry, respectively, while the experimental ones have no symmetry probably due to some perturbation in crystals. The optimized geometrical parameters of **1**—**3** are in good agreement with experimental results and a trend that the stepwise replacement of a chloride ligand by a butyl group resulted in the elongation of the Sn–N and Sn–Cl is well reproduced.

This tendency may be understood based on the orbital interactions between fragments Tp* and $SnCl_{3-n}Bu_n$. The schematic orbital interactions are drawn in Fig. 6. The fragments of $(N)_3$ group in the Tp* ligand have three group orbitals suitable to form the Sn–N bonds; one a and two e symmetry orbitals. The a and e orbitals of Sn in the $SnCl_3$ fragment of **1** are mainly composed of the p_z and the d_{yz} and d_{xz} orbitals, respectively. The orbitals having the same symmetry interact to form three bonding and three *anti*-bonding orbitals. The substitution of a chloride atom with a butyl group destabilizes the Sn orbitals since the orbitals have larger *anti*-bonding coupling with carbon atom orbitals of the butyl group than that of the chlorine atom orbital. The energy difference, therefore, between interacting partner orbitals of $(N)_3$ becomes larger and the bonding interaction becomes weak. Thus the Sn–N bond is weaker in the alkyl substituted tin compound than that of unsubstituted one. In the complex **3** all interacting orbitals of Sn are more destabilized than those in **2**. Hence the Sn–N bonds become weaker and the Sn–N bond distances become longer than those in **2**.

Among the three Sn–N bonds, the bonds *trans* to the butyl group are more elongated than that *trans* to the chloride atom in **3**, while the opposite tendency is found in **2**. The e symmetry orbital in **1** splits into the a′ and the b′ symmetry orbitals in **2** and **3**. The b′ symmetry orbital is higher in energy than the a′ symmetry orbital. Therefore, the orbital interaction between the b′ orbital of Sn and the e symmetry orbital of $(N)_3$ is weaker than that between the a′ symmetry orbital of Sn and the e symmetry orbital of $(N)_3$. In complex **2**, the interaction of b′ symmetry orbitals which contributes to the Sn–N(*trans* to Cl) bonding interaction resulted in the longer Sn–N(*trans* to Cl) bond distances. Similarly, the disadvantage of the b′ symmetry orbital interaction results in the longer Sn–N(*trans* to Bu) bond distances in **3**.

The positive charge on the tin atom increases with an increase in the number of the butyl groups bound to the tin atom; the net charge is +1.782 in **1**, +1.844 in **2**, and +1.878 in **3**, respectively. The butyl ligand acts as a stronger σ-donor than the chloride ligand in the Tp* organotin compounds. A substitution of a chloride ligand with a butyl group decreases the positive charge on the tin atom. On the other hand, the butyl ligand weakens the other coordination bonds and suppresses the electron donation from the other ligands. This effect increases the positive charge on the tin atom. The calculated results suggest that the latter may be larger than the former in the organotin complexes.

Some comment is needed on the geometries and the net charge on the tin atom of the organotin compounds obtained from the MNDO calculations, which gave the sorter Sn–C and Sn–Cl bonds and the longer Sn–N bonds than those from the ab initio MO calculations. The positive charge on the tin atom decreases going from **1** to **3**; +1.023 in **1**, +0.875 in **2**, and +0.078 in **3**, respectively; this tendency is the opposite of the result from the ab initio MO calculations.

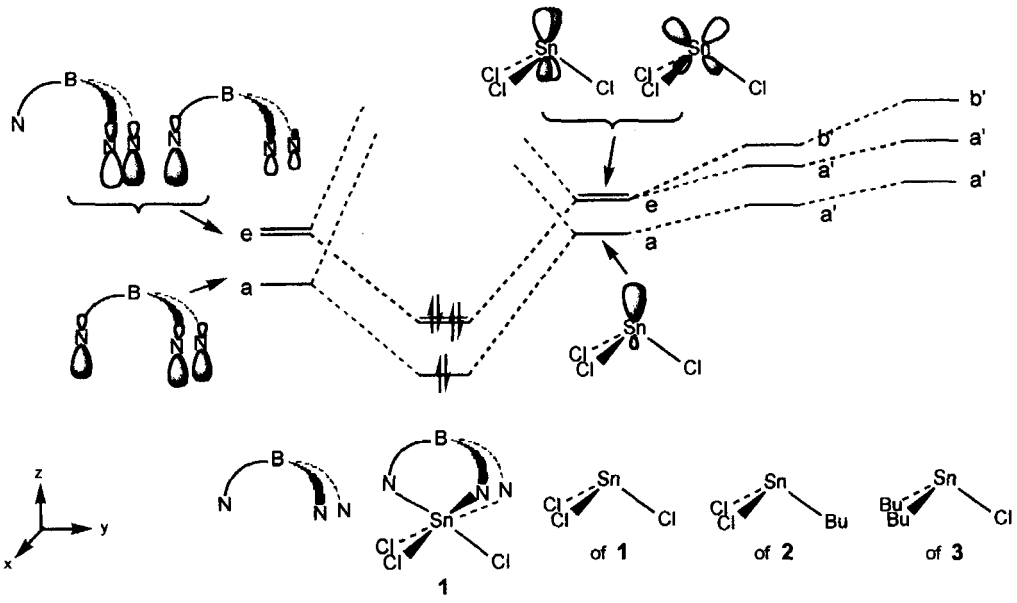

Fig. 6. Schematic orbital interactions for **1**—**3**.

This suggests that the strength of the σ-donor of butyl ligand is overestimated by the MNDO method.

Synthesis of Tp* Complexes. On the basis of the above findings, we applied the compound **3** to prepare Tp* complexes of Group 4—6 metals.

Group 4 Metals. The reaction of **3** and $ZrCl_4$ in preparative scale produced **4** in 79% yield (Eq. 2). This convenient synthetic method has an advantage compared with the previous reactions of KTp* and $ZrCl_4$ in dichloromethane which required the separation of the product from waste alkaline salts and, critically, two molar amounts of $ZrCl_4$ to achieve a high yield.[20] Reaction of $TiCl_4$ with an equimolar amount of **3** in toluene gave a mono-Tp* titanium complex, [Tp*$TiCl_3$] (**7**)[33] in 89% yield as orange powder after a simple rinse to remove $SnCl_2Bu_2$. We can prepare a Tp* hafnium complex, [Tp*$HfCl_3$] (**8**) in a similar manner, though the only reported hafnium complex is [TpHf(Cp)Cl_2].[34] Complex **8** was obtained in 90% yield by treating [$HfCl_4(THF)_2$] with an equimolar amount of **3** in toluene under reflux, while the reaction at room temperature did not proceed at all. In contrast, the reaction of $HfCl_4$ with **3** in toluene gave only trace to negligible yield of **8**, presumably due t o the low solubility of $HfCl_4$ in toluene. Spectral data indicated the octahedral geometry of these Tp* complexes.

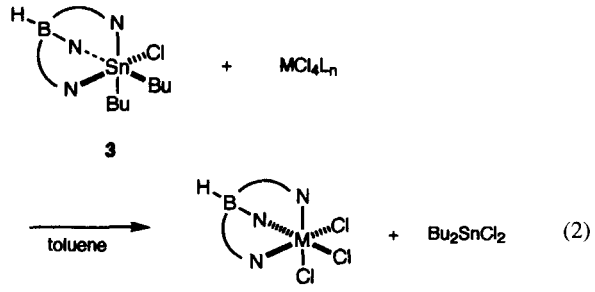

Group 5 Metals. We preliminary reported mono Tp* complexes of niobium and tantalum;[19] the reaction of **3** with a stoichiometric amount of [$NbCl_4(THF)_2$] or [$NbCl_5(OEt)_2$] in toluene gave [Tp*$NbCl_3$] (**9**), while the similar reaction with $TaCl_5$ gave [Tp*$TaCl_3$][$TaCl_6$] (**10**) (Chart 3). The previous syntheses of $TpMCl_n$-type complexes of niobium and tantalum using alkaline metal Tp compound have mostly resulted in tcomplex mixtures and crystallographically characterized $TpMCl_n$-type complexes of niobium and tantalum have never been reported.[35,36]

We applied our method to prepare Tp* complexes of vanadium. A vanadium(III) complex [$VCl_3(THF)_3$] readily reacted with an equimolar amount of **3** in THF to give a mono-Tp* vanadium complex [Tp*VCl_2(THF)] (**11**) in 73% yield (Eq. 3), though a Tp analog was reported.[37] The green crystals of **11** became opaque upon exposure to argon atmosphere due to the release of the coordinated THF. The THF molecule is easily substituted by the other donor molecule DMAP (= 4-dimethylaminopyridine). Treatment of **11** with DMAP in THF at room temperature afforded [Tp*VCl_2(DMAP)] (**12**) as green crystals in good yield (Eq. 3), characterized by X-ray analysis.

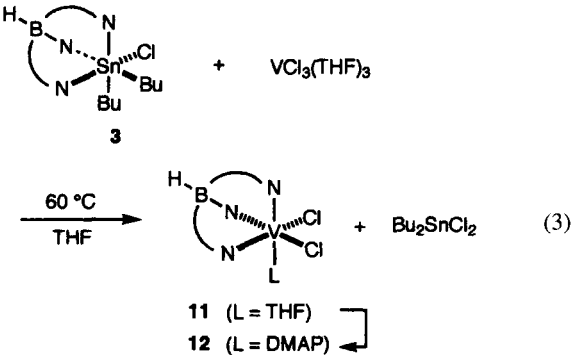

Moreover, compound **3** is an useful reagent to prepare a Tp* vanadium(V) complex possessing an imido ligand, though the related imido complexes have been prepared by the metathesis reaction of VCl_3(=NR) with KTp* and were found to be a catalyst for the polymerization of ethylene and propylene upon combing with MAO.[38] Treatment of VCl_3(=$NC_6H_3Me_2$-2,6) with an equimolar amount of **3** in hexane at 60 °C for 12 h resulted in the formation of [Tp*VCl_2(=$NC_6H_3Me_2$-2,6)] (**13**) in 84% yield (Eq. 4). The diamagnetic vanadium(V) d^0 complex **13** can be characterized by spectral data and X-ray analysis. The ^{1}H NMR spectrum of **13** shows two sets of the proton signals due to the pyrazolyl moieties of the coordinated Tp* in the expected integral ratio of 2 : 1. Two nonequivalent methyl signals and three different aromatic protons due to one 2,6-xylyl moiety indicate the presence of a mirror plane passing through the aromatic plane. The electronic spectrum of **13** showed a characteristic intense band at λ_{max} = 412 nm attributed to a LMCT band from a filled N(pπ) orbital to an empty V(dπ^*) orbital.[39]

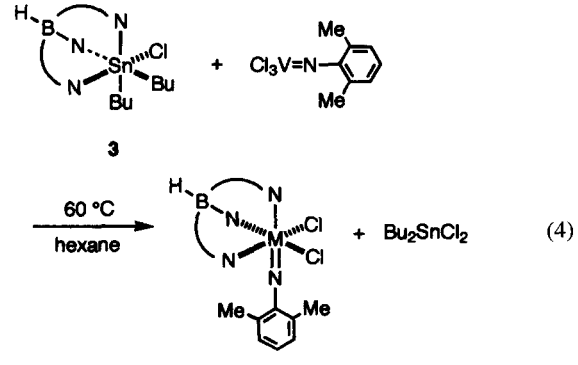

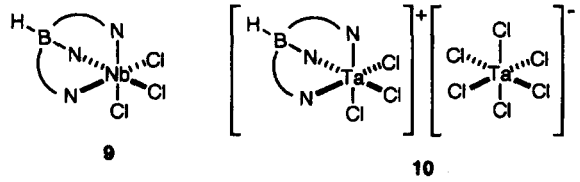

Chart 3.

Chromium Complexes. Hydrotris(pyrazolyl)borate complexes of chromium have rarely been reported,[40—44] despite there are many Tp complexes of molybdenum and tungsten.[1] Compound **3** has proven to be an effective Tp* transfer reagent for the synthesis of a mono-Tp* chromium complex. The reaction of $[CrCl_3(THF)_3]$ with an equimolar amount of **3** in THF afforded $[Tp^*CrCl_2(THF)]$ (**14**) as green crystals in 90% yield (Eq. 5). The IR spectrum of **14** showed an strong absorption at 860 cm^{-1}, indicating a THF molecule coordinated to the chromium center.

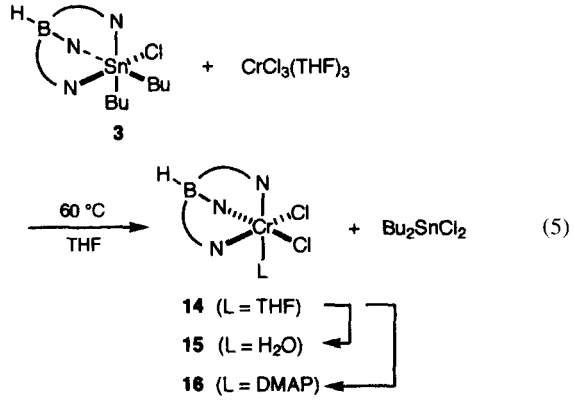

The THF molecule of **14** can be replaced by water. Recrystallization of **14** from aqueous THF gave an aqua complex $[Tp^*CrCl_2(H_2O)]$ (**15**) in quantitative yield (Eq. 5). The water molecule bound to the metal was revealed by IR spectroscopy (a sharp absorption band at 3300 cm^{-1}). The THF molecule of **14** can also be replaced by an amine such as DMAP; treatment of **14** with an equimolar amount of DMAP led to the formation of $[Tp^*CrCl_2(DMAP)]$ (**16**) in 87% yield. The structures of these chromium complexes were determined by combustion analyses and X-ray studies.

Structural Features of Tp* Complexes of Zirconium, Hafnium, Vanadium, and Chromium. The solid state structures of **4**, **8**, **12**, **13**, **15**, and **16** were determined by single-crystal X-ray crystallography, and their ORTEP drawings and selected bond lengths and angles are shown in Figs. 7, 8, 9, 10, 11, and 12 and Tables 3, 4, and 5,

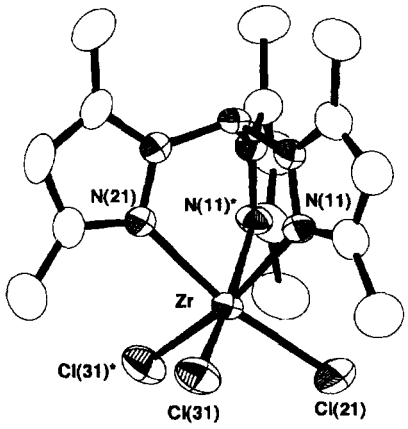

Fig. 7. ORTEP drawing of complex **4** with the numbering scheme. Hydrogen atoms are omitted for clarity.

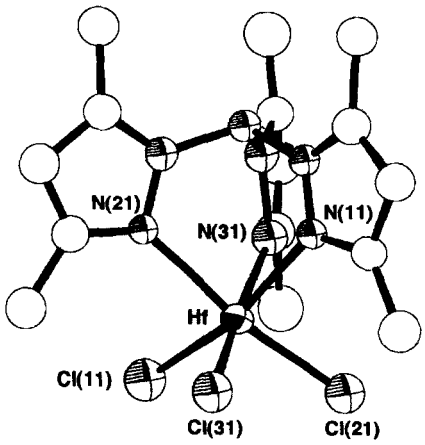

Fig. 8. ORTEP drawing of **8** with the numbering scheme. Hydrogen atoms are omitted for clarity.

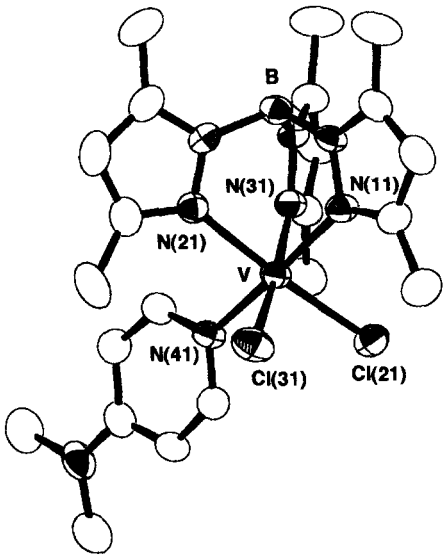

Fig. 9. ORTEP drawing of **12** with the numbering scheme. Hydrogen atoms are omitted for clarity.

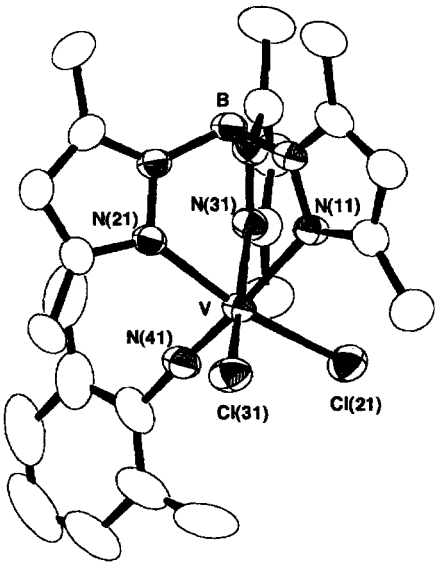

Fig. 10. ORTEP drawing of **13** with the numbering scheme. Hydrogen atoms are omitted for clarity.

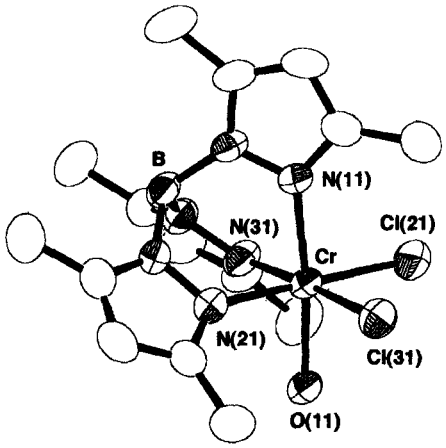

Fig. 11. ORTEP drawing of one of the two crystallographically independent molecules of **15** with the numbering scheme. Hydrogen atoms are omitted for clarity.

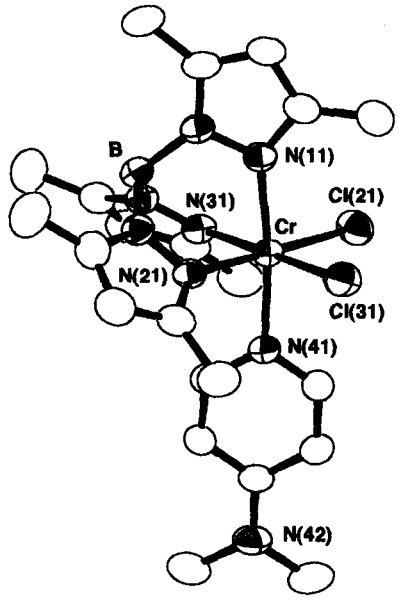

Fig. 12. ORTEP drawing of **16** with the numbering scheme. Hydrogen atoms are omitted for clarity.

respectively; we also determined the crystal structure of **7**, but it has recently been reported.[45] As expected from the analytical and spectroscopic data, these are discrete mononuclear molecules having a facially coordinating tridentate Tp* ligand and three other ligands and they adopt the distorted octahedral geometry; the three N–M–N angles within the Tp*M fragment are, as usual, less than 90° and the three *trans* N–M–L angles deviate from ideal 180°, as a consequence of the chelate nature of the Tp* ligand.

Complexes **4** and **8** essentially have the same structure due to lanthanoid contraction. The average Zr–N bond distance (2.282 Å) of **4** is slightly shorter than that (2.311 Å) found for $[Tp^*ZrCl(OC_6H_3Me_2\text{-}2,6)_2]$,[46] where π-donation from the oxygen atom to the metal center resulted in the elongation of the Zr–N bond *trans* to the aryloxo ligand.

Six-coordinated Tp* complexes of vanadium and chromium have the same geometry around the metal center, if they have the same ligand. Two DMAP adducts **12** and **16** are isomorphous; both vanadium and chromium centers adopt the octahedral geometry comprised of a facial $(N)_3$

Table 3. Selected Bond Distances and Angles for Tp* Complexes of Zirconium and Hafnium

	4	**8**
	Bond distances (Å)	
M–N(11)	2.280(4)	2.38(2)
M–N(21)	2.286(6)	2.288(8)
M–N(31)	—	2.15(2)
M–Cl(11)	—	2.352(7)
M–Cl(21)	2.399(2)	2.399(3)
M–Cl(31)	2.385(2)	2.415(6)
	Bond angles (deg)	
N(11)–M–N(21)	80.9(1)	82.3(5)
N(11)–M–N(31)	—	80.8(3)
N(11)–M–Cl(11)	—	167.7(4)
N(11)–M–Cl(21)	91.0(1)	95.3(4)
N(11)–M–Cl(31)	90.9(1)	87.8(4)
N(21)–M–N(31)	—	82.5(6)
N(21)–M–Cl(11)	—	85.9(4)
N(21)–M–Cl(21)	169.5(1)	168.1(3)
N(21)–M–Cl(31)	90.7(1)	94.9(4)
N(31)–M–Cl(11)	—	94.2(5)
N(31)–M–Cl(21)	—	85.6(5)
N(31)–M–Cl(31)	—	168.5(5)
Cl(11)–M–Cl(21)	—	95.5(2)
Cl(11)–M–Cl(31)	—	96.8(1)
Cl(21)–M–Cl(31)	96.30(6)	96.7(1)

a) For complex **8**, N(31) = N(11)*, Cl(11) = Cl(31)*.

Table 4. Selected Bond Distances and Angles for **12** and **13**

	12	**13**
	Bond distances (Å)	
V–N(11)	2.124(4)	2.226(2)
V–N(21)	2.118(4)	2.112(3)
V–N(31)	2.155(4)	2.120(3)
V–N(41)	2.135(4)	1.687(3)
V–Cl(21)	2.345(2)	2.303(1)
V–Cl(31)	2.328(2)	2.290(1)
	Bond angles (deg)	
N(11)–V–N(21)	88.0(2)	84.90(10)
N(11)–V–N(31)	87.1(1)	83.01(9)
N(11)–V–N(41)	175.7(2)	177.3(1)
N(11)–V–Cl(21)	92.1(1)	88.30(7)
N(11)–V–Cl(31)	92.6(1)	85.68(7)
N(21)–V–N(31)	83.7(2)	83.83(10)
N(21)–V–N(41)	89.9(2)	92.6(1)
N(21)–V–Cl(21)	173.5(1)	170.04(7)
N(21)–V–Cl(31)	91.5(1)	88.75(7)
N(31)–V–N(41)	89.0(2)	95.7(1)
N(31)–V–Cl(21)	89.8(1)	89.57(8)
N(31)–V–Cl(31)	175.2(1)	166.97(7)
N(41)–V–Cl(21)	89.6(1)	94.03(10)
N(41)–V–Cl(31)	91.3(1)	95.37(10)
Cl(21)–V–Cl(31)	94.97(6)	96.56(4)
V–N(41)–C(41)	—	175.7(3)

Table 5. Selected Bond Distances and Angles for Chromium Complexes **15** and **16**

	15-I	**15-II**	**16**
		Bond distances (Å)	
Cr–N(11)	2.051(4)	2.045(4)	2.072(4)
Cr–N(21)	2.073(6)	2.070(6)	2.083(5)
Cr–N(31)	2.069(5)	2.082(5)	2.094(5)
Cr–O(11)	2.017(4)	2.007(4)	—
Cr–N(41)	—	—	2.087(4)
Cr–Cl(21)	2.315(2)	2.309(3)	2.315(2)
Cr–Cl(31)	2.319(2)	2.319(2)	2.321(2)
		Bond angles (deg)	
N(11)–Cr–N(21)	87.3(2)	88.8(2)	86.9(2)
N(11)–Cr–N(31)	89.0(2)	87.7(2)	86.9(2)
N(11)–Cr–O(11)	173.8(2)	174.4(2)	—
N(11)–Cr–N(41)	—	—	173.0(2)
N(11)–Cr–Cl(21)	99.3(2)	93.4(2)	92.3(1)
N(11)–Cr–Cl(31)	92.6(1)	93.3(1)	92.9(1)
N(21)–Cr–N(31)	87.4(2)	86.5(2)	88.1(2)
N(21)–Cr–O(11)	87.7(2)	88.1(2)	—
N(21)–Cr–N(41)	—	—	88.6(2)
N(21)–Cr–Cl(21)	178.1(2)	177.3(1)	178.8(1)
N(21)–Cr–Cl(31)	91.6(1)	90.5(1)	90.0(1)
N(31)–Cr–O(11)	87.0(2)	87.5(2)	—
N(31)–Cr–N(41)	—	—	87.6(2)
N(31)–Cr–Cl(21)	90.8(2)	92.0(2)	91.0(1)
N(31)–Cr–Cl(31)	177.0(1)	176.9(2)	178.1(2)
O(11)–Cr–Cl(21)	91.6(1)	89.6(2)	—
O(11)–Cr–Cl(31)	90.1(1)	91.4(1)	—
N(41)–Cr–Cl(21)	—	—	92.1(1)
N(41)–Cr–Cl(31)	—	—	92.4(1)
Cl(21)–Cr–Cl(31)	90.16(7)	90.90(7)	90.87(7)

coordination of the Tp* ligand, two chloride atoms and one nitrogen atom of DMAP. The average V–N bond distance (2.132 Å) of the Tp* ligand in **12** is longer than that (2.083 Å) found for **16**, and the bond distance (2.135(4) Å) of V–N(41) in **12** is also longer than that (2.087(4) Å) of Cr–N(41) in **16**. An aqua chromium complex **15**, which crystallized as two crystallographically-independent molecules **15-I** and **15-II**, has a water ligand and its structure is quite normal.

The whole structural feature of a vanadium(V) imido complex **13** is quite similar to that of reported complexes, $[Tp^*V(=NC_6H_3^iPr_2\text{-}2,6)Cl_2]$[38] and $[TpV(=N^tBu)Cl_2]$[38] along with an oxovanadium analog $[Tp^*V(=O)Cl(O^tBu)]$.[47] The bond distance (1.687(3) Å) of V–N(41) and the bond angle (175.7(3)°) of V–N(41)–C(41) in **13** were comparable with those observed in $[Tp^*VCl_2(=NC_6H_3^iPr_2\text{-}2,6)]$ (1.693(4) Å and 173.7(3)°, respectively). For the Tp* ligand of **13**, the V–N(*trans* to the imido ligand) bond distance (2.226(2) Å) is longer than the V–N(*cis* to the imido ligand) distances (2.112(3) and 1.120(3) Å) due to the multiple bond character of the V–N(41), whose distance is significantly shorter than the bond distance (2.135(4) Å) of V–N(41) found for the DMAP adduct **12**.

Conclusion

The reactivity of Tp* organotin compounds of general formula $[Tp^*SnCl_{3-n}Bu_n]$ (**1**: $n = 0$; **2**: $n = 1$; **3**: $n = 2$) toward halometal complexes of early transition metals has been elucidated by using the test reaction with an equimolar amount of $ZrCl_4$ to produce $[Tp^*ZrCl_3]$ (**4**). As a result, **3** has proved to be a useful reagent as mono Tp* complexes of various early transition metals. Structural analyses of these organotin compounds indicated that the complex **3** has a longer average Sn–N bond than those of complexes **1** and **2**, presumably due to the strong *trans*-influence of the butyl ligand. Such a tendency has been understood on the basis of the ab initio calculations. Thus, we applied compound **3** for the preparation of a variety of Tp* complexes of Group 4 and 5 metals and chromium, whose structures were characterized by spectral measurements and by X-ray crystallographic analyses. Although our synthetic method required pre-preparation of the organotin compound **3**, this has remarkable advantages to prepare early transition metal halo complexes under mild conditions and to isolate the product only by a simple operation.

Experimental

General. All manipulations involving air- and moisture-sensitive organometallic compounds were carried out using standard Schlenk techniques under argon. Dichloromethane was washed with water and then distilled under argon after drying over P_2O_5. THF, toluene, and hexane were dried over sodium benzophenone ketyl or P_2O_5, and then distilled before use. Compounds

[Tp*SnCl$_3$] (**1**), [Tp*SnCl$_2$Bu] (**2**), and [Tp*SnClBu$_2$] (**3**) were prepared according to the literature procedures.[21] SnCl$_4$, BuSnCl$_3$, and Bu$_2$SnCl$_2$ were purchased from Nacalai Tesque, Inc.

^{1}H (270 MHz) and ^{119}Sn (110 MHz) NMR spectra were measured on a JEOL JNM-GSX-270 spectrometer. All ^{1}H NMR chemical shifts were reported in ppm relative to protio impurity resonance as follows: chloroform-*d*, singlet at 7.26 ppm; benzene-d_6, singlet at 7.20 ppm, dichloromethane-d_2, triplet at 5.35 ppm. Other spectra were recorded by the use of the following instruments: IR, JASCO FT/IR-120; UV/vis spectra, JASCO V-570; ESR spectra, Bruker EMX 10/12. Elemental analyses were performed on a Perkin–Elmer 2400 microanalyzer. All melting points were measured in sealed tubes and were not corrected.

Reaction of ZrCl$_4$ with Organotin Tp* Compounds. To a suspension of ZrCl$_4$ in CDCl$_3$ (0.01 mmol mL^{-1}) at ambient temperature was added an equimolar amount of an organotin Tp* compound. The reaction mixture was stirred rapidly for 10 min, and then the mixture was quickly transferred into an NMR tube via a syringe. The tube was cooled below −40 °C and then sealed. The ^{1}H NMR spectrum of the reaction mixture containing [Tp*ZrCl$_3$] (**4**) as a product was recorded at −40 °C.

Preparation of [Tp*ZrCl$_3$] (4). To a suspension of ZrCl$_4$ (138.3 mg, 0.512 mmol) in dichloromethane (5 mL) was added dropwise **3** (289.5 mg, 0.512 mmol) at room temperature. After the reaction mixture was stirred for 2 h, the resulting off-white solid of **4** was filtered off, and then washed with a portion of hexane. Recrystallization from a mixture of dichloromethane and hexane at −20 °C gave **4** (106.6 mg, 79% yield) as colorless crystals, mp > 300 °C (decomp). ^{1}H NMR (CDCl$_3$) δ = 2.40 (s, 9 H), 2.68 (s, 9 H), 5.84 (s, 3 H). IR (nujol/KBr) 2563 (ν_{B-H}) cm^{-1}. Anal. Calcd for C$_{15}$H$_{22}$BCl$_3$N$_6$Zr: C, 36.41; H, 4.48; N, 16.99%. Found: C, 36.03; H, 4.51; N, 16.67%.

Preparation of [Tp*TiCl$_3$] (7). To a solution of TiCl$_4$ (284.5 mg, 1.5 mmol) in toluene (15 mL) at room temperature was added a solution of **3** (848.4 mg, 1.5 mmol) in toluene (10 mL) via syringe. The color of the reaction mixture gradually turned red accompanied by the precipitation of reddish product while stirring for 12 h at room temperature. All volatiles were removed under reduced pressure, and then the resulting residue was washed with toluene (20 mL) and hexane (40 mL), giving orange solids of **7** (598.3 mg, 89% yield). Analytically pure **7** was obtained by the recrystallization from a mixture of dichloromethane and hexane at −20 °C, mp > 300 °C (decomp). ^{1}H NMR (CDCl$_3$) δ = 2.38 (s, 9 H), 2.76 (s, 9 H), 5.84 (s, 3 H). IR (nujol/KBr) 2557 (ν_{B-H}) cm^{-1}. Anal. Calcd for C$_{15}$H$_{22}$BCl$_3$N$_6$Ti: C, 39.91; H, 4.91; N, 18.62%. Found: C, 39.60; H, 4.86; N, 18.42%.

Preparation of [Tp*HfCl$_3$] (8). A reaction mixture of **3** (698.4 mg, 1.08 mmol) and [HfCl$_4$(THF)$_2$] (501.8 mg, 1.08 mmol) in toluene (20 mL) was heated at reflux for 12 h. The reaction mixture was concentrated under reduced pressure. The resulting off-white solids were filtrated off and then were washed with toluene to give **8** (565.2 mg, 90% yield). Recrystallization from a mixture of dichloromethane and hexane at −20 °C gave an analytical pure **8**, mp > 300 °C. ^{1}H NMR (CDCl$_3$) δ = 2.40 (s, 9 H), 2.69 (s, 9 H), 5.88 (s, 3 H). IR (nujol/KBr) 2563 (ν_{B-H}) cm^{-1}. Anal. Calcd for C$_{15}$H$_{22}$BCl$_3$HfN$_6$: C, 30.95; H, 3.81; N, 14.44%. Found: C, 30.60; H, 3.83; N, 14.27%.

Preparation of [Tp*VCl$_2$(THF)] (11). A mixture of **3** (216.8 mg, 0.38 mmol) and [VCl$_3$(THF)$_3$] (143.2 mg, 0.38 mmol) in THF (20 mL) was heated at 60 °C for 12 h. The solvent was removed under reduced pressure. The residue was washed with hexane. Recrystallization of the product from a mixture of THF and hexane at −20 °C gave **11** (137.2 mg, 73% yield) as green crystals, mp 292—295 °C (decomp). IR (nujol/KBr) 2544 (ν_{B-H}) cm^{-1}. Anal. Calcd for C$_{19}$H$_{30}$BCl$_2$N$_6$OV: C, 46.46; H, 6.16; N, 17.11%. Found: C, 45.80; H, 5.99; N, 17.34%.

Preparation of [Tp*VCl$_2$(DMAP)] (12). 4-Dimethylaminopyridine (7.4 mg, 0.06 mmol) was added to a solution of **11** (29.9 mg, 0.06 mmol) in THF (2 mL). The reaction mixture was stirred for 1 h at room temperature. After removal of volatiles under reduced pressure, the product residue was crystallized from a mixture of dichloromethane and hexane, giving **12** as green crystals (34.1 mg, 89% yield), mp > 300 °C (decomp). IR (nujol/KBr) 2549 (ν_{B-H}) cm^{-1}. Anal. Calcd for C$_{22}$H$_{32}$BCl$_2$N$_8$V(CH$_2$Cl$_2$): C, 44.12; H, 5.47; N, 17.90%. Found: C, 44.02; H, 5.48; N, 17.76%.

Preparation of [Tp*VCl$_2$(=NC$_6$H$_3$Me$_2$-2,6)] (13). A solution of VCl$_3$(=NC$_6$H$_3$Me$_2$-2,6) (115.5 mg, 0.42 mmol) and **3** (236.3 mg, 0.42 mmol) in hexane (10 mL) was heated at 60 °C for 12 h. The resulting dark green solids were filtrated off and then washed with hexane to leave **13** (190.0 mg, 84% yield). Recrystallization from a mixture of dichloromethane and hexane at room temperature gave an analytically pure **13** as black crystals, mp 242—246 °C (decomp). ^{1}H NMR (C$_6$D$_6$) δ = 1.92 (s, 3 H), 2.04 (s, 6 H), 2.18 (s, 3 H), 2.46 (s, 6H), 3.11 (s, 3 H), 3.95 (s, 3 H), 5.45 (s, 2 H), 5.61 (s, 1 H), 6.39—6.42 (m, 1 H), 6.60—6.75 (m, 1 H), 6.85—6.95 (m, 1 H). UV/vis (CH$_2$Cl$_2$) λ_{max} 412 nm (ε = 1.4×10^4 M^{-1} cm^{-1}) (1 M = 1 mol dm^{-3}). IR (nujol/KBr) 2547 (ν_{B-H}) cm^{-1}. Anal. Calcd for C$_{23}$H$_{31}$BCl$_2$N$_7$V: C, 51.33; H, 5.81; N, 18.22%. Found: C, 50.77; H,5.89; N, 18.22%.

Preparation of [Tp*CrCl$_2$(THF)] (14). To a solution of [CrCl$_3$(THF)$_3$] (325.6 mg, 0.85 mmol) in THF (20 mL) was added dropwise a solution of **3** (480.7 mg, 0.85 mmol) in THF (10 mL). The reaction mixture was heated at 60 °C for 12 h. The resulting dark green solids were filtrated off and then washed with hexane to leave **14**. Recrystallization from a mixture of THF and hexane at −20 °C afforded **14** as green crystals (376.6 mg, 90% yield), mp 251—253 °C (decomp). IR (nujol/KBr) 2540 (ν_{B-H}), 860 (ν_{C-O-C}) cm^{-1}. Anal. Calcd for C$_{19}$H$_{30}$BCl$_2$CrN$_6$O: C, 46.37; H, 6.14; N, 17.07%. Found: C, 47.00; H, 6.40; N, 17.44%.

Preparation of [Tp*CrCl$_2$(H$_2$O)] (15). Complex **14** (95.9 mg, 0.19 mmol) was dissolved in wet THF (0.5 mL), and then slow evaporation of the solvent under air gave **15** as green crystals (66.6 mg) in 80% yield, mp 215—218 °C (decomp). IR (nujol/KBr) 3330 (ν_{O-H}), 2560 (ν_{B-H}) cm^{-1}. Anal. Calcd for C$_{15}$H$_{24}$BCl$_2$CrN$_6$(C$_4$H$_8$O)$_{1.5}$: C, 46.17; H, 6.64; N, 15.38%. Found: C, 46.00; H, 6.24; N, 15.56%.

Preparation of [Tp*CrCl$_2$(DMAP)] (16). To a solution of **14** (56.4 mg, 0.11 mmol) in THF (20 mL) was added dropwise a solution of 4-dimethylaminopyridine (13.4 mg, 0.11 mmol) in THF (5 mL). The reaction mixture was stirred at room temperature for 2 h, and then the resulting green powder was collected by filtration and washed with hexane. The product was extracted with THF, and then recrystallization from THF at room temperature afforded **16** as dark green crystals (54.2 mg, 87% yield), mp > 300 °C. IR (nujol/KBr) 2540 (ν_{B-H}), 1620 (ν_{N-C}) cm^{-1}. UV/vis (CH$_2$Cl$_2$) λ_{max} 362 nm (ε = 708 M^{-1} cm^{-1}). Anal. Calcd for C$_{22}$H$_{32}$BCl$_2$CrN$_8$(C$_4$H$_8$O)$_{0.5}$: C, 49.85; H, 6.27; N, 19.38%. Found: C, 49.64; H, 6.80; N, 18.92%.

Spectral Simulations. The simulated spectra were calculated with use of the gNMR computer program. The experimental and simulated spectra were matched by visual comparison of the spectra. The Eyring plot of ln (k/T) vs. 1/T was made on a computer using a standard least-squares analysis. The slope y intercept of the line were obtained directly from the calculator.

Computational Methods. Ab initio Calculations. The ab initio MO calculations were performed on the DEC/Alpha400 workstation using Gaussian 94.[30]

MNDO Calculations. The semiempirical calculations were carried out using standard MNDO method and parameters, as implemented in the MOPAC 93 package of computer programs. The MNDO calculations were performed on the SX-4 computer at Computation Center Osaka University.

Crystallographic Data Collections and Structure Determination of 1—3, 4, 8, 12, 13, 15, and 16. Data Collection. All suitable crystals were mounted in glass capillaries under argon atmosphere. Data for each complex were collected by a Rigaku AFC-7R diffractometer with a graphite monochromated Mo $K\alpha$ (λ = 0.71069 Å) radiation and a 12 kW rotating anode generator. The incident beam collimator was 1.0 mm and the crystal to detector distance was 285 mm. Cell constants and an orientation matrix for data collection, obtained from a least-squares refinement using the setting angles of 25 carefully centered reflections corresponded to the cells with dimensions listed in Tables 6 and 7, where details of the data collection were summarized. The weak reflections ($I < 10\sigma(I)$) were rescanned (maximum of 2 rescans) and the counts were accumulated to assure good counting statistics. Stationary background counts were recorded on each side of the reflection. The ratio of peak counting time to background counting time was 2 : 1. Three standard reflections were chosen and monitored every 150 reflections.

Data Reduction. An empirical absorption correction based on azimuthal scans of several reflections was applied. The data were corrected for Lorentz and polarization effects. The decay of intensities of three representative reflections was −0.31% for **1**, −0.29% for **2**, −1.46% for **3**, −3.07% for **4**, −0.42% for **8**, −0.25% for **13**, −24.03% for **15**, and −2.55% for **16**, and thus linear correction factors were applied to the decay of these observed data. Complex **12** showed no decay.

Structure Determination and Refinement. All calculations were performed using a TEXSAN crystallographic software package, and illustrations were drawn with ORTEP. Crystallographic calculations were performed on IRIS Indigo workstation. The structure was solved by convenient direct methods; complexes **1**, **2**, **3**, **4**, and **15** by SHELXS 86,[48] complex **8** by a Patterson method (SAPI),[49] and complexes **12**, **13**, and **16** by a Patterson method (PATTY).[50] A series of standard full matrix least-squares refinement and Fourier synthesis revealed the remaining atoms. For complexes **1**—**3**, **4**, and **8**, all hydrogen atoms were placed by the calculated position (C–H and B–H = 0.95 Å). For complexes **12**, **13**, **15**, and **16**, all hydrogen atoms were found in a difference Fourier map. For three tin complexes **1**—**3**, the structure was refined on F^2 and the function minimized was $[\sum w(F_o^2 - F_c^2)]$. The function R_1 and wR_2 were $(\sum||F_o| - |F_c||)/\sum|F_o|$ and $[\sum w(F_o^2 - F_c^2)^2/\sum w(F_o^4)]^{1/2}$, respectively. For complexes **4**, **8**, **12**, **13**, **14**, and **15**, measured nonequivalent reflections with $I > 3.0\sigma(I)$ were used for the structure determination. In the subsequent refinement the function $\sum w(|F_o| - |F_c|)^2$ was minimized, where $|F_o|$ and $|F_c|$ are the observed and calculated structure factors amplitudes, respectively. The agreement indices are defined as $R = \sum||F_o| - |F_c||/\sum|F_o|$ and $R_w = [\sum w(|F_o| - |F_c|)^2/\sum w(|F_o|)^2]^{1/2}$. Atomic positional param-

Table 6. Crystal and Refinement Data for **1**—**3**

Complex	**1**	**2**	**3**
Formula	$C_{15}H_{22}BCl_3N_6Sn$	$C_{19}H_{31}BCl_2N_6Sn$	$C_{23}H_{40}BClN_6Sn$
Formula weight	522.24	543.90	565.56
Cryst system	Monoclinic	Monoclinic	Monoclinic
Space group	$P2_1$ (#4)	$P2_1/c$ (#14)	$P2_1$ (#4)
a/Å	8.128(2)	12.284(5)	8.360(2)
b/Å	14.195(4)	16.207(7)	18.329(3)
c/Å	9.213(1)	24.720(4)	9.400(2)
β/deg	100.30(1)	96.26(2)	104.45(2)
Z	2	8	2
V/Å^3	1045.9(4)	4892(3)	1394.8(5)
D_{calcd}/g cm^{-3}	1.658	1.477	1.347
Radiation	Mo $K\alpha$	Mo $K\alpha$	Mo $K\alpha$
Reflections measd	$+h, +k, \pm l$	$+h, +k, \pm l$	$+h, +k, \pm l$
Crystal size/mm	0.2×0.3×0.3	0.1×0.3×0.6	0.2×0.5×0.5
Abs. coeff/cm^{-1}	16.16	12.80	10.32
Scan mode	ω–2θ	ω–2θ	ω–2θ
Temp/°C	20	20	20
$2\theta_{max}$/deg	55.0	55.0	55.1
Data collected	2671	11714	3512
Unique data	2506 (R_{int}=0.031)	11200 (R_{int}=0.043)	3299 (R_{int}=0.032)
No. of observation ($I>2\sigma(I)$)	2158	7274	2157
No. of variables	234	559	283
R_1 ($I>2\sigma(I)$)	0.026	0.041	0.039
wR_2 ($I>2\sigma(I)$)	0.059	0.095	0.076
R_1 (all data)	0.039	0.093	0.093
wR_2 (all data)	0.063	0.112	0.090
GOF on F^2	1.053	1.013	1.013
Δ/e Å^{-3}	0.356 (max) −0.611 (min)	0.595 (max) −0.808 (min)	0.376 (max) −0.517 (min)

Table 7. Crystal and Refinement Data of Tp^* Complexes of **4**, **8**, **12**, **13**, **15**, and **16**

Complex	**4**	**8**	**12**	**13**	**15**	**16**
Formula	$C_{15}H_{22}BCl_3N_6Zr$	$C_{15}H_{22}BCl_3N_6Hf$	$C_{22}H_{32}BCl_2N_8V(CH_2Cl_2)$	$C_{23}H_{31}BCl_2N_7V$	$C_{19}H_{36}BCl_2CrN_6O_{2.5}$	$C_{22}H_{32}BCl_2CrN_8(OC_4H_8)$
Formula weight	494.77	582.04	626.14	538.20	522.24	614.37
Cryst system	Monoclinic	Monoclinic	Monoclinic	Monoclinic	Triclinic	Triclinic
Space group	$P2_1/m$ (#11)	$P2_1$ (#4)	$P2_1$ (#4)	$P2_1/c$ (#14)	$P\bar{1}$ (#2)	$P\bar{1}$ (#2)
a/Å	8.138(2)	8.141(1)	9.850(2)	14.897(2)	12.674(3)	10.670(1)
b/Å	14.191(7)	14.210(3)	14.317(3)	9.968(2)	20.102(4)	14.892(2)
c/Å	9.320(2)	9.293(2)	10.670(2)	18.873(2)	12.146(4)	10.599(2)
α/deg					99.72(2)	92.92(1)
β/deg	100.07(2)	100.12(1)	93.04(1)	105.361(8)	111.48(2)	99.37(1)
γ/deg					73.07(2)	99.42(1)
Z	2	2	2	4	4	2
V/Å^3	1059.8(5)	1058.3(3)	1502.6(4)	2702.5(6)	2748(1)	1634.1(4)
D_{calcd}/g cm^{-3}	1.550	1.826	1.415	1.323	1.262	1.249
Radiation	Mo $K\alpha$	Mo $K\alpha$	Mo $K\alpha$	Mo $K\alpha$	Mo $K\alpha$	Mo $K\alpha$
Reflections measd	$+h, +k, \pm l$	$+h, +k, \pm l$	$+h, +k, \pm l$	$+h, +k, \pm l$	$+h, \pm k, \pm l$	$-h, \pm k, \pm l$
Crystal size/mm	0.2 × 0.4 × 0.7	0.3 × 0.3 × 0.3	0.5 × 0.2 × 0.5	0.4 × 0.3 × 0.3	0.6 × 0.5 × 0.4	0.5 × 0.4 × 0.2
Abs. coeff/cm^{-1}	9.08	53.10	6.47	5.14	6.38	5.45
Scan mode	ω–2θ	ω–2θ	ω–2θ	ω–2θ	ω–2θ	ω–2θ
Temp/°C	20	20	20	20	20	20
$2\theta_{max}$/deg	55.0	55.0	55.0	55.0	55.0	55.0
Data collected	2716	2710	3805	6821	13201	7930
Unique data	2544 (R_{int} = 0.025)	2544 (R_{int} = 0.023)	3605 (R_{int} = 0.013)	6577 (R_{int} = 0.017)	12629 (R_{int} = 0.045)	7494 (R_{int} = 0.059)
No. of observation ($I > 3\sigma(I)$)	1762	2199	2849	4030	6090	5055
No. of variables	133	109	333	307	565	327
R	0.047	0.043	0.041	0.045	0.062	0.070
R_w	0.062	0.058	0.047	0.053	0.083	0.087
GOF	1.79	1.96	1.67	1.82	1.82	3.91
Δ/e Å^{-3}	0.64 (max) −0.68 (min.)	1.39 (max) −1.86 (min)	0.38 (max) −0.30 (min.)	0.29 (max) −0.35 (min)	1.03 (max) −0.64 (min)	1.41 (max) −0.72 (min)

eters for the non-hydrogen atoms of all complexes are given in Supporting Information.

Crystallographic data have been deposited at the CCDC, 12 Union Road, Cambridge CB2 1EZ, UK and copies can be obtained on request, free of charge, by quoting the publication citation and the deposition numbers 144538-144545. The data are also deposited as Document No. 73041 at the Office of the Editor of Bull. Chem. Soc. Jpn.

We appreciate Dr. T. Yamagata (Osaka University) for his guidance to X-ray analysis. This work was financially supported by a Grant-in-Aid for Scientific Research on Priority Area from the Ministry of Education, Science, Sports and Culture. K.M. appreciates the partial financial support from the Yamada Science Foundation.

Supporting Information

Details of crystal structure determination of **1**—**3**, **4**, **8**, **12**, **13**, **15**, and **16**; final positional parameters, final thermal parameters, bond distances and angles together with drawings showing the atom-numbering scheme (104 pages).

References

1 S. Trofimenko, "Scorpionates-The Coordination Chemistry of Polypyrazolylborate Ligands," Imperial College Press, London (1999).

2 S. Trofimenko, *Prog. Inorg. Chem.*, **34**, 115 (1986).

3 A. Shaver, "Comprehensive Coordination Chemistry," ed by G. Wilkinson, R. D. Gillard, and J. A. McCleverty, Pergamon, Oxford (1987), Vol. 2.

4 N. Kitajima and W. B. Tolman, *Prog. Inorg. Chem.*, **43**, 419 (1995).

5 G. Parkin, *Adv. Inorg. Chem.*, **42**, 291 (1995).

6 G. H. Maunder, A. Sella, and D. A. Tocher, *J. Chem. Soc., Chem. Commun.*, **1994**, 2689.

7 D. L. Reger, C. A. Swift, and L. Lebioda, *J. Am. Chem. Soc.*, **105**, 5343 (1983).

8 D. L. Reger, C. A. Swift, and L. Lebioda, *Inorg. Chem.*, **23**, 349 (1984).

9 J. M. Boncella, M. L. Cajigal, and K. A. Abboud, *Organometallics*, **15**, 1905 (1996).

10 A. Antinolo, F. Carrillo-Hermosilla, J. Fernandez-Baeza, M. Lanfranchi, A. Lara-Sanchez, A. Oterro, E. Palomarez, M. A. Pellinghelli, and A. M. Rodriguez, *Organometallics*, **17**, 3015 (1998).

11 M. Etienne, P. S. White, and J. L. Templeton, *Organometallics*, **10**, 3801 (1991).

12 M. Etienne, F. Biasotto, and R. Mathieu, *J. Chem. Soc., Chem. Commun.*, **1994**, 1661.

13 M. Etienne, *Organometallics*, **13**, 410 (1994).

14 M. Etienne, B. Donnadieu, R. Mathieu, J. F. Baeza, F. Jalón, A. Otero, and M. E. Rodrigo-Blanco, *Organometallics*, **15**, 4597 (1996).

15 M. Etienne, R. Mathieu, and B. Donnadieu, *J. Am. Chem. Soc.*, **119**, 3218 (1997).

16 A. M. Cardoso, R. J. H. Clark, and S. Moorhouse, *J. Chem. Soc., Dalton Trans.*, **1980**, 1156.

17 T. Okamoto, H. Yasuda, A. Nakamura, Y. Kai, N. Kanehisa, and N. Kasa, *J. Am. Chem. Soc.*, **110**, 5008 (1988).

18 C. H. Dungan, W. Maringgele, A. Meller, K. Niedenzu, H. Noeth, J. Serwatowska, and J. Serwatowski, *Inorg. Chem.*, **30**, 4799 (1991).

19 K. Mashima, T. Oshiki, and K. Tani, *Organometallics*, **16**, 2760 (1997).

20 D. L. Reger and M. E. Tarquini, *Inorg. Chem.*, **21**, 840 (1982).

21 G. F. Lobbia, F. Bonati, P. Cecchi, A. Lorenzotti, and C. Pettiari, *J. Organomet. Chem.*, **403**, 317 (1991).

22 G. G. Lobbia, G. Valle, S. Calogero, P. Cecchi, C. Santini, and F. Marchetti, *J. Chem. Soc., Dalton Trans.*, **1996**, 2475.

23 B. K. Nicholson, *J. Organomet. Chem.*, **265**, 153 (1984).

24 G. F. Lobbia, S. Calogero, B. Bovio, and P. Cecchi, *J. Organomet. Chem.*, **440**, 27 (1992).

25 G. G. Lobbia, P. Cecchi, S. Calogero, G. Valle, M. Chiarini, and L. Stievano, *J. Organomet. Chem.*, **503**, 297 (1995).

26 G. G. Lobbia, P. Cecchi, R. Spagna, M. Colapietro, A. Pifferi, and C. Pettinari, *J. Organomet. Chem.*, **485**, 45 (1995).

27 S. Calogero, L. Stievano, G. G. Lobbia, A. Cingolani, P. Cecchi, and G. Valle, *Polyhedron*, **14**, 1731 (1995).

28 O.-S. Jung, J. H. Jeong, and Y. S. Sohn, *J. Organomet. Chem.*, **399**, 235 (1990).

29 S. Trofimenko, *J. Am. Chem. Soc.*, **91**, 3183 (1969).

30 P. Meakin, S. Trofimenko, and J. P. Jesson, *J. Am. Chem. Soc.*, **94**, 5677 (1972).

31 Y. D. Ward, L. A. Villanueva, G. D. Allred, S. C. Payne, M. A. Semones, and L. S. Liebeskind, *Organometallics*, **14**, 4132 (1995).

32 M. J. Frisch, G. W. Trucks, H. B. Schlegel, P. M. W. Gill, B. G. Jonson, M. A. Robb, J. R. Cheeseman, T. Keith, G. A. Petersson, J. A. Montgomery, K. Raghavachari, M. A. Al-Laham, V. G. Zakrzewski, J. V. Ortiz, J. B. Foresman, J. Cioslowski, B. B. Stefanov, A. Nanayakkara, M. Challacombe, C. Y. Peng, P. Y. Ayala, W. Chen, M. W. Wong, J. L. Andres, E. S. Replogle, R. Gomperts, R. L. Martin, D. J. Fox, J. S. Binkley, D. J. Defrees, J. Baker, J. P. Stewart, M. Head-Gordon, C. Gonzalez, and J. A. Pople, "Gaussian 94," Gaussian, Inc., Pittsburgh, PA (1995).

33 J. K. Kouba and S. S. Wreford, *Inorg. Chem.*, **15**, 2313 (1976).

34 R. A. Kresinski, C. J. Jones, and J. A. McCleverty, *Polyhedron*, **9**, 2185 (1990).

35 L. G. Hubert-Pfalzgraf and M. Tsunoda, *Polyhedron*, **2**, 203 (1983).

36 D. C. Bradley, M. B. Hursthouse, J. Newton, and N. P. C. Walker, *J. Chem. Soc., Chem. Commun.*, **1984**, 188.

37 L. E. Manzer, *J. Organomet. Chem.*, **102**, 167 (1975).

38 S. Scheuer, J. Fischer, and J. Kress, *Organometallics*, **14**, 2627 (1995).

39 D. D. Devore, J. D. Lichtenhan, F. Takusagawa, and E. A. Maatta, *J. Am. Chem. Soc.*, **109**, 7408 (1987).

40 M. J. Abrams, R. Faggiani, and C. J. L. Lock, *Inorg. Chem. Acta*, **106**, 69 (1985).

41 J. H. MacNeil, W. C. Watkins, M. C. Baird, and K. F. Preston, *Organometallics*, **11**, 2761 (1992).

42 V. Skagestad and M. Tilset, *J. Am. Chem. Soc.*, **115**, 5077 (1993).

43 J. Sundermeyer, J. Putterlik, M. Foth, J. S. Field, and N. Ramesar, *Chem. Ber.*, **127**, 1201 (1994).

44 C.-H. Li, J.-D. Chen, L.-S. Liou, and J.-C. Wang, *Inorg. Chim. Acta*, **269**, 302 (1998).

45 A. Antinolo, F. Carrillo-Hermosilla, A. E. Corrochano, J. Fernandez-Baeza, M. Lanfranchi, A. Oterro, and M. A. Pellinghelli, *J. Organomet. Chem.*, **577**, 174 (1999).

46 R. A. Kresinski, L. Isam, T. A. Hamor, and C. J. Jones, *J. Chem. Soc., Dalton Trans.*, **1991**, 1835.

47 C. J. Carrano, M. Mohan, S. M. Holmes, R. de la Rosa, A. Butler, J. M. Charnock, and D. Garner, *Inorg. Chem.*, **33**, 646 (1994).

48 G. M. Sheldrick, "SHELXS-86. Program for the Solution of Crystal Structures," University of Göttingen, Germany (1985).

49 F. Hai-Fu, "SAPI91, Program for Crystal Structure Determination," Rigaku Corp., Tokyo, Japan (1991).

50 J. Karle, *Acta Crystallogr., Sect. B*, **B24**, 182 (1968). "The DIRDIF program system, Technical Report of the Crystallography Laboratory," University of Nijmegen, The Netherlands. "*teXsan*: Single Crystal Structure Analysis Software, Version 1.6f (1993)," Molecular Structure Corporation, The Woodlands, TX 77381.